# Non-destructive multi-sensor core logging allows rapid imaging, measurement of bulk density and estimation of ice content in permafrost cores

Joel Pumple [1, *], Alistair Monteath [1], Jordan Harvey [1], Mahya Roustaei [1, 3], Alejandro Alvarez [1], Casey
Buchanan [1, 2] and Duane Froese [1, *]

[1] Department of Earth and Atmospheric Sciences, University of Alberta, Edmonton, Canada
[2] Yukon University, Whitehorse, YT
[3] Department of Civil Engineering, Ghent University, Ghent, Belgium

Correspondence to: Joel Pumple (*pumple@ualberta.ca*) or Duane Froese (duane.froese@ualberta.ca)

10  **Abstract.** Permafrost cores provide physical samples that can be used to measure the characteristics of frozen ground. Measurement of core physical properties, however, are typically destructive and time intensive. In this study, multi-sensor core logging (MSCL) is used to provide a rapid, high-resolution, non-destructive method to image and collect the physical properties of permafrost cores, allowing the visualization of cryostructures, measurement of bulk density and magnetic susceptibility, and estimation of volumetric ice content. Six permafrost cores with differing properties were analyzed using

15  MSCL and compared with established destructive analyses to assess the potential of this instrument both in terms of accuracy and relative rate of data acquisition. A calibration procedure is presented for gamma ray attenuation from a $^{137}$Cs source that is specific to frozen core materials. This accurately measures bulk density over the wide range of material densities found in permafrost. MSCL bulk density data show strong agreement with destructive analyses based on discrete sample measurements. Bulk density data from the gamma attenuation, along with soil density measurements for different

20  sediment types, are used to estimate volumetric ice content. The results show strong agreement with destructive analyses, illustrating that MSCL can provide accurate non-destructive estimates of ice contents and provide a digital archive of permafrost cores for future applications.

## 1 Introduction

Permafrost cores are typically collected from remote locations at great expense. Despite the considerable cost involved in the
recovery of permafrost cores, most methods are destructive and rarely preserve physical or digital archives for future work.
Typically, permafrost samples are qualitatively described in the field based on visible or nonvisible ice content (Pihlainen
and Johnson, 1963; Linell and Kaplar, 1966; ASTM D4083-89, 2016). These descriptions may include cryostructures of the
ice and sediment, and a subset of these observations may be combined with destructive analyses to quantify volumetric ice
content, excess ice, gravimetric moisture content, and soil organic matter (Pihlainen and Johnston, 1963; Andersland and
Ladanyi, 1994; Kokelj and Burn, 2003; French and Shur, 2010; Stephani et al., 2010). These properties can be used to
estimate thaw potential or for the interpretation of cryostratigraphy. The accurate measurement of these variables is
important for designing climate-resilient infrastructure and predicting the impacts of permafrost thaw. A second concern
with permafrost characterization arises because increasing air temperatures and thawing permafrost mean that permafrost
landscapes are rapidly changing. This transformation of permafrost regions emphasizes the need to archive material that may
not be available for future research (Jorgenson et al., 2010; Throop et al., 2012), or may be appropriate for complementary
applications.

In recent decades there have been advances in using laboratory based non-destructive methods for measuring the physical
properties of frozen materials, including gamma attenuation (e.g. Zhou et al., 2014; Lenz et al., 2015), ultrasonic methods
(Liu et al., 2023), nuclear magnetic resonance (Kleinberg and Griffin, 2005; Kruse and Darrow, 2017), and computed
tomography scanning (e.g. Calmels and Allard, 2004; Carbonneau et al., 2011; Darrow and Lieblappen, 2020). This study
investigates the use of multi-sensor core logging (MSCL) to characterize permafrost cores. The MSCL is well established in
its application for marine sediments (Weber et al., 1997; Gunn and Best, 1998), landslide assessments (Hunt et al., 2011;
Vardy et al., 2012), contaminated sediments (Kuras et al., 2016), and environmental studies of lake sediments (Smol et al.,
2001; Fortin et al., 2013). However, to our knowledge, the application of MSCL on frozen materials has not been developed.
Here, we use MSCL systems to measure the physical properties of frozen cores with gamma ray attenuation, non-contact
resistivity, magnetic susceptibility, and high-resolution line-scan imagery. The goals of this paper are to first develop
calibration methods for gamma attenuation density determination based on physical principles and present a preferred
method specific to frozen materials; second, to analyze six permafrost cores with differing physical properties to test the
suitability of MSCL for non-destructive characterization; finally, we compare these results with destructive measurements at
similar spatial scales on discrete sediment samples.

## 2 Methods and materials

### 2.1 Multi Sensor Core Logger (MSCL)

This study uses a Geotek (U.K.) MSCL in the Permafrost ArChives Science (PACS) Laboratory at the University of Alberta,
Canada. The MSCL is a floor-mounted, automated logging system that passes core along a track, either below or between
55 analytical sensors (Fig. 1). This system can be used to analyze whole or split cores up to 150 cm long, with outer diameters
less than 15 cm. The PACS Laboratory MSCL is equipped with two magnetic susceptibility instruments (Bartington Loop
sensor for whole cores and a contact magnetic susceptibility sensor for split core), a high-resolution line-scan camera, a
Caesium-137 ($^{137}$Cs) gamma ray source and detector, and a non-contact resistivity sensor. In this study, we used the MSCL
split core configuration. The core boat used for both the cores and calibration pieces is a 10 cm diameter PVC pipe with
60 cores sitting in an open style half pipe and the calibration piece in a whole pipe with a viewing window to allow for
submersion of the calibration piece within water/ice (Fig. 1).

The MSCL system within the PACS Laboratory is located in a space kept at 23 °C. Although the PACS Laboratory has cold
rooms and walk-in freezer spaces, in the design phase, the decision was made to develop a core scanning method that could
be completed at room temperature. This provided savings in construction costs and is likely to reduce maintenance
65 time/costs compared with a cold room installation where higher moisture and condensation could impact electronics and
camera. As a result, we developed a method for working on frozen cores that would maintain the integrity of the cores
through analysis at room temperature.

### 2.1.1 Gamma Attenuation Operating Principles

The MSCL is equipped with a Caesium-137 ($^{137}$Cs) gamma ray source and detector for measuring the attenuation of gamma
70 rays through the core. These measurements are also referred to as gamma ray attenuation porosity evaluator (GRAPE)
density measurements (Evans, 1965), and are commonly used in marine and lacustrine sediment cores (Weber et al., 1997;
Geotek, 2021). In its simplest form, a gamma ray source passes a beam of collimated gamma rays through a 2.5 or 5 mm
aperture through the centre of the core. Photons passing through the core are detected at the sensor, while some are
attenuated, largely by Compton scattering, resulting in partial energy loss. When other variables, including the gamma
75 source intensity, Compton attenuation coefficient and core thickness are known, the degree of energy loss can be used to
calculate bulk sediment density (Geotek, 2021). As the density of ice (0.9 g/cm$^3$) is substantially lower than minerals that
typically make up sediment cores (e.g., quartz 2.65 g/cm$^3$), density changes in ice-rich permafrost cores are principally
driven by sediment porosity/organic content and the abundance of ice within the sediments.

4

**2.1.2 PACS Laboratory permafrost core operating protocol**

80    The methods described here have been developed to provide accurate core bulk density measurements while mitigating the risk of thaw during analysis. These include experiments designed to identify suitable gamma ray attenuation analytical times while minimizing core exposure at temperatures >0 °C.

Accurate gamma ray attenuation measurements require a minimum of approximately 100,000 counts per measurement at the gamma ray detector (Geotek per comms, 2022). This is achieved through longer measurement times (up

85    to 30 seconds) for calibration. To assess the minimum count time required to meet this threshold, three permafrost cores with different sediment properties and ice contents were analyzed using 30 second, 10 second, 5 second and two second count times. The 5 mm aperture was used to maximize counts per second. Our results showed that a five second count time produced consistent results (>100,000 counts per measurement) that agreed well with longer count times (10 second and 30 second) and were adopted for subsequent measurements. This approach resulted in an average acquisition time of 2-3

90    cm/minute using a 5 mm aperture and 5 mm sampling resolution. After removal from a -25 °C freezer, the internal temperature of a test half core increased to ~ -12 °C during a 30-minute acquisition. This approach met the requirements to accurately measure sediment densities of our samples. Denser or thicker cores would require longer analytical time for similar counts. As well as this, count times required to reach minimum counts at the detector will vary over time as the Caesium-137 source decays.

95    **2.1.3 Development of calibration standards for frozen materials**

As gamma bulk density, to our knowledge, has not previously been used to analyze permafrost cores via MSCL, several experiments were completed to develop a calibration protocol. To calculate bulk density from gamma ray attenuation, the MSCL uses a stepped aluminum calibration block of known thickness and density. This is analyzed using a fixed count time (typically 30 seconds) at the gamma detector and runs across the length of the calibration block, including a small section

100    outside the calibration block to capture the core casing/core boat and background material. In common practice, the background material is air for dry cores and water for saturated cores. The density and thickness of the aluminum block, along with the known density of the background (air, water, or ice as we discuss), are then used to convert the resulting counts per second into $g/cm^3$. In our initial experiments, we used the default aluminum calibration block from the manufacturer; however, due to the length of the steps (3 cm), the determination of the average counts between steps was

105    difficult to consistently capture using the shorter count times. These inconsistencies were further affected by stainless steel screws at either end of the aluminum block. To meet these challenges, we constructed a new calibration block based on the manufacturer's design, but with longer steps (6 cm rather than 3 cm) and no screws (Fig. 2).

Permafrost samples typically include variable ice content and minimal free water below ~ -10 °C. The calibration approach outlined by the manufacturer did not span the range of densities and materials encountered in the frozen sediments

110    (ice, 0.9 $g/cm^3$ to clast-rich diamict, >2.4 $g/cm^3$). When analyzing unfrozen sediment cores, calibration of bulk density

5

typically uses the aluminum calibration piece submerged in water as pore-spaces are assumed to be saturated. As water is denser than ice, this leads to a potential source of bias in measuring the density of ice-rich materials (e.g. peat and ice lenses), which lay outside of the calibration range. To extend the calibration range, and account for the density differences between ice and water, the newly-developed stepped standard piece was submerged in water and frozen prior to calibration (Fig. 2). This frozen calibration piece produced results more comparable to frozen materials of known density (e.g. pure ice and peat that are expected to have densities ~0.9 g/cm$^3$). Unsurprisingly, the offset between frozen and unfrozen calibration was greatest in ice-rich materials. Figure 2 shows a piece of foam on the left side of the calibration piece (to keep it level) and highlights the depth of the water/ice surrounding the calibration piece (blue dashed line). The foam piece results in a local density low or high depending on the surrounding medium. It should also be noted that the accuracy of the calibration, when using this frozen calibration piece, was sensitive to the depth of the surrounding ice. The goal was to have the ice level with the flat surface of the calibration piece to minimize variability. Repeat analyses were completed on frozen half cores with a 5 second count time and 5 mm gamma source aperture to quantify uncertainty in the density measurement. The measured uncertainty based on 15 repeat measurements is ± 0.05 g/cm$^3$.

Beam spreading below the gamma source aperture results in the beam diameter increasing from 5 mm at the aperture to ~ 10 mm at the core surface, and likely expands further to ~15 mm at the detector. This cone shape causes an edge effect that leads to bulk density measurements decreasing at or near any core breaks or sharp density contrasts (eg. top and bottom of a core or the calibration piece; Figure 2). The gamma attenuation data from the bottom and top of the cores has been edited to remove edge affected data.

### 2.1.2 Magnetic Susceptibility (Mag Sus)

The MSCL is equipped with two magnetic susceptibility instruments: a Bartington MS2E point sensor and a Bartington MS2C loop sensor (160 mm diameter). In this paper, the results from the Bartington MS2E point sensor are used as the measurement field is finer (approximately 2 cm) than the Bartington MS2C loop sensor (approximately 7 cm). This resolution increases the likelihood of capturing sharp cryostratigraphic transitions (e.g. ice lenses). When analysing core materials, the instruments were zeroed and calibrated against instrument specific Bartington standards before and following the analyses. Bartington MS2E point sensor measurements follow the same central vertical transect as the gamma density measurements allowing comparison between the two datasets.

### 2.1.3 Non-Contact Resistivity (NCR)

The Non-Contact Resistivity (NCR) sensor induces a high frequency magnetic field in the core that in turn induces electrical currents which are inversely proportional to resistivity. These are measured using receiver coils and compared with identical receiver coils operating in the air (Geotek, 2021). In permafrost cores, these electrical currents are likely to be altered by the differing abundance of ice and water because of the variable conductivities of these two materials.

The NCR instrument was tested on frozen materials, but was strongly affected by the temperature of the cores, and attempts to analyze frozen cores were hampered by substantial analytical drift between measurements. Similar problems were encountered during studies of Antarctic Ocean cores by Niessen et al. (2007), who did not consider the majority of their

145    NCR results reliable. An attempt was made to mitigate this issue by 'cooling' the sensor using a synthetic frozen core, however, drift during the analyses was considered too great. These issues meant that despite the considerable potential for measuring unfrozen water content in permafrost cores using NCR, at present, the temperature sensitivity of the instrument makes it unsuitable for this application. The NCR sensor is not discussed further.

### 2.1.4 Line-scan imagery

150    Split cores were photographed using the line-scan camera equipped on the MSCL. The camera uses a Canon 50 mm lens focused through a thin viewing window in the lighting box. The resolution of the resulting images ranges from 100-micron pixels (low resolution setting) to 25 micron pixels (high resolution setting), and all images are exported as 48-bit RGB TIFF files. Moisture scavenging from the room caused some cores to build up ice on the core surfaces when scanned at ≤-20 °C, despite the low humidity conditions which are common in Alberta, Canada. This led to overexposure and poor image quality

155    in some sections. To mitigate this problem cores were warmed to -5 °C before imaging which improved image quality in both low- and high-resolution scans. This meant that core images and physical properties were measured in separate core runs, to minimize sample thaw potential during analyses.

### 2.2 Physical density measurements

To independently assess density measurements made using gamma attenuation, both volumetric and gravimetric methods

160    were completed on the same cores. The cores were subsampled as close as possible to the transect analyzed by the MSCL gamma density instrument (Fig. 3).

Destructive analyses for bulk density, volumetric and excess ice contents follow methods described by Kokelj and Burn (2003), but are modified to provide higher resolution for comparison with the MSCL data. Instead of using whole (10 cm) core segments, we used the cuboid method, as described by Bandara et al. (2019), which is based on precisely measured

165    cuboids sampled throughout core segments. The cuboids in this study were processed in a walk-in freezer held at -7 °C. The first step was to remove material from the outer core edges that may have been thawed during coring or affected by sample storage. Core segments were split lengthwise using a rock saw equipped with a 35 cm diameter diamond cutting wheel (Fig. 4A). Cuboid aliquots were cut from half of the split core while the other half is retained as an archive (Fig. 4A). The rounded edges were removed from the half core to reveal an internal slab (Fig. 4B). For this study a duplicate set of cuboids were

170    collected by cutting the internal slab in half (Fig. 4C). Approximately 3 cm$^3$ aliquots were subsampled from the cores to ensure that cuboids did not fracture or disintegrate during sampling because of the lower ice content (Fig. 4D). Digital calipers (±0.01 mm) and a digital analytical balance (±0.01 g precision) were used to measure physical dimensions and mass, respectively, to calculate the bulk density (Fig. 4E & 4F). The cuboids were then thawed at room temperature for 24 hours in

175 glass beakers covered in parafilm to minimize evaporative loss (Fig. 4G & 4H). Any excess moisture was removed from the beakers containing the thawed samples and the sample weight was recorded again to calculate excess moisture content (Fig. 4I). The cuboids were then dried in an oven for 24 hours at 105 °C and reweighed to calculate both volumetric ice content and gravimetric moisture content (Fig. 4J & 4K). Finally, the remaining dried material was heated at 550 °C for 4 hours to determine the percent organic content via loss on ignition (LOI) (Fig. 4L; Heiri et al., 2001).

## 2.3 Volumetric ice content estimates

180 We estimate the ice content of cores from the bulk density following the approach used by Lin et al. (2020). This approach relates volumetric ice content and bulk density as:

$$\rho = \frac{m}{V} = \frac{m_s + m_i + m_w + m_a}{V} = \frac{\rho_s v_s + \rho_i v_i + \rho_w v_w + \rho_a v_a}{V} \qquad (1)$$

Where $\rho$ is density (g/cm$^3$), m is mass (g), and V is volume (cm$^3$). Subscripts *s, i, w,* and *a* represent soil particles, ice content (both segregated ice and pore ice), unfrozen water, and air, respectively. V is the volume of the permafrost sample and is 185 assumed as 1 unit volume so the above simplified to:

$$\rho = \rho_s v_s + \rho_i v_i + \rho_w v_w + \rho_a v_a \qquad (2)$$

And by considering the mean volumetric content of unfrozen water and air equal to 1 and 2%, respectively, as well as 0.9 and 1 g/cm$^3$ for the density of ice and water, and ignoring the density of air, the equation is simplified to:

$$\rho = 2.04 v_s + 0.9 v_i + 0.02 \qquad (3)$$

190 Lin et al. (2020) use a value of 2.04 g/cm$^3$ for the soil specific density of homogeneous permafrost samples from the Qinghai-Tibet Plateau, while in this study, specific densities for each core are measured using the cuboid method, with most ranging from 1.4 to 2.6 g/cm$^3$ (Table 1). The largest source of uncertainty using this approach is the assumed soil density value.

## 2.4 Materials

195 Six permafrost cores that represent common materials encountered in permafrost regions were analyzed in this study. Each core segment was selected based on relatively simple cryostructures to minimize lateral heterogeneity (Table 1).

## 3 Results

### 3.1 Ice-wedge (BH19-204):

This core consists of sediment-poor ground ice with subvertical foliations. This represents a typical ice-wedge core from 200 permafrost affected regions (Murton and French, 1994). The ice-wedge core was scanned on the MSCL for bulk density, but was not processed via the cuboid method due to the high ice volume and lack of sediment in the core (Fig. 5). The mean

density based on gamma attenuation is $0.90 \pm 0.03$ g/cm$^3$, while the average, minimum and maximum magnetic susceptibility values for this core are -1.55 SI x 10$^{-5}$, -3.64 SI x 10$^{-5}$, and 2.38 SI x 10$^{-5}$, respectively.

### 3.2 Ice-rich silt (BH18-211):

205  This core consists of ice-rich, organic sandy silt dominated by a wavy-micro-lenticular cryostructure and a single ice layer ~1 cm thick. Both MSCL and cuboid data were collected from the core (Fig. 6). The average density for the gamma attenuation and cuboid method are $1.27 \pm 0.1$ g/cm$^3$ and $1.24 \pm 0.1$ g/cm$^3$, respectively, and consistent through the core. The volumetric ice content for the two datasets shows strong agreement apart from the ice-poor regions in the core where the MSCL method estimates lower values relative to the cuboid data. The average, minimum, and maximum magnetic

210  susceptibility values for this core are 13.44 SI x 10$^{-5}$, 0.79 SI x 10$^{-5}$, and 29.23 SI x 10$^{-5}$, respectively.

### 3.3 Transition core (BH12F-138):

This core contains a sharp transition between an overlying ice-rich silty peat and an underlying ice-poor inorganic silt with micro-lenticular cryostructures. Bulk density from the gamma attenuation and cuboid methods in the top half of the core (ice-rich silty peat) are $0.98 \pm 0.02$ g/cm$^3$ and $1.02 \pm 0.03$ g/cm$^3$, respectively (Fig. 7). The mean density for the gamma

215  attenuation and cuboid method in the bottom half of the core (ice-poor inorganic silt) are $1.31 \pm 0.14$ g/cm$^3$ and $1.32 \pm 0.25$ g/cm$^3$, respectively. Both the gamma attenuation and cuboid bulk density data resolve the transition. The two datasets track well except for the high-density peak (volumetric ice content low) in the lower half (below 8 cm depth) of the core which is missed by the 2 cm resolution cuboid data. The average, minimum, and maximum magnetic susceptibility values for this core are 32.08 SI x 10$^{-5}$, -0.66 SI x 10$^{-5}$, and 151.64 SI x 10$^{-5}$, respectively.

220  ### 3.4 Diamicton (BS19-3-6):

BS19-3-6 is an ice-rich diamicton with suspended and crustal cryostructures. The mean density for the gamma attenuation and cuboid methods are $1.45 \pm 0.11$ g/cm$^3$ and $1.46 \pm 0.11$ g/cm$^3$, respectively (Fig. 8). Overall, this core shows good agreement between the MSCL and cuboid methods. The datasets differ notably from 2-4 cm depth and 10-12 cm depth where the gamma attenuation dataset shifts toward lower density values. The cause of these differences is discussed in Sect.

225  4.1. The mean, minimum, and maximum magnetic susceptibility values for this core are 36.83 SI x 10$^{-5}$, 6.42 SI x 10$^{-5}$, and 230.34 SI x 10$^{-5}$, respectively.

### 3.5 Ice-poor silt (BH20B-337):

This core consists of ice-poor sandy silt with a massive/structureless cryostructure (i.e. lacking visible ice). Silt in this core is relatively homogeneous, with the mean density for the gamma attenuation and cuboid method being $1.75 \pm 0.07$ g/cm$^3$ and

230  $1.85 \pm 0.05$ g/cm$^3$, respectively (Fig. 9). The cuboid data shows minimal variability throughout the core; however, the higher-resolution gamma attenuation data shows greater variability in bulk density. Overall, the gamma attenuation bulk

9

density data agrees with the cuboid data. Similarly, the MSCL volumetric ice content agrees with the cuboid data. The mean, minimum, and maximum magnetic susceptibility values for this core are 354.14 SI x $10^{-5}$, 285.89 SI x $10^{-5}$, and 409.29 SI x $10^{-5}$, respectively. This core contains the highest magnetic susceptibility values of all the cores in the study.

235 **3.6 Ice-rich peat (DH13-589):**

The peat core consists of homogenous organics with an organic-matrix cryostructure displaying some visible ice within pore spaces. The mean density for the gamma attenuation and cuboid method are $0.9 \pm 0.01$ g/cm$^3$ and $0.91 \pm 0.08$ g/cm$^3$, respectively (Fig. 10). The gamma attenuation data agree well with the cuboid measurements and highlight the ability of the gamma attenuation to capture subtle changes in the density of frozen peat. The mean, minimum, and maximum magnetic 240 susceptibility values for this core are -1.43 SI x $10^{-5}$, -2.19 SI x $10^{-5}$, and -0.73 SI x $10^{-5}$, respectively.

**4 Discussion**

The non-destructive MSCL method provides a rapid method to collect core images, bulk density, magnetic susceptibility and data to estimate volumetric ice contents from a variety of permafrost materials. Cores analyzed in this study were selected to represent the diverse physical properties and materials encountered in permafrost regions. With the exception of the 245 diamicton core (BS19-3-6), the cores were selected based on their assumed low degree of lateral heterogeneity along the cores central vertical axes representing the main sample locations. The non-destructive MSCL density data are plotted versus the cuboid density data in Figure 11. This figure also shows a strong agreement between the methods illustrating the reliability of the MSCL method to non-destructively collect physical properties of permafrost cores (Fig. 11).

In addition to bulk density data, volumetric ice content data was measured using the cuboid method and estimated 250 using gamma attenuation bulk density following Lin et al. (2020). However, rather than a single value for the soil particle density, we measured the average soil density for each core using the cuboid data. These measured values showed considerable variation (ca. 1.4-2.5 g/cm3), but with additional measurements of more permafrost types, reliable estimates for different sediment types can likely be established. An added challenge to reliable estimates of ice content is the need for careful core preparation of frozen materials such that thickness is constant and core samples sit in contact with the core boat 255 as discussed in Sect. 4.1. Overall, the gamma attenuation and cuboid ice content results show strong agreement and demonstrate the potential for systematic and reliable estimation of ground ice content within permafrost cores non-destructively (Fig. 12).

**4.1 Density Variability and Lateral Heterogeneity**

Variations in measured densities of permafrost cores may reflect real heterogeneities in physical properties, or alternatively, 260 artifacts introduced due to core preparation or mounting of frozen materials. For example, the diamicton core (BS19-3-6) has

a strong lateral heterogeneity in composition that is highlighted by the offset between the cuboid sample locations and the central path of the MSCL gamma beam (Fig. 8). From 2-4 cm depth in the diamicton core, the MSCL dataset records a large difference in bulk density, and as a result, also in estimated ice content relative to the cuboid data. (Fig. 3). These cores were selected in part because of their assumed lack of lateral heterogeneity to minimize the impact when comparing the results

265   between the destructive and non-destructive methods. The diamicton example highlights the importance of that consideration. At this depth in the core a clast caused a local density high and a corresponding low in ice content in the cuboid sample data. This high density and low ice content area was not observed in the gamma attenuation data reflecting the lateral offset in data collection location along the core.

One challenge in using the MSCL for frozen cores occurs because frozen cores behave rigidly in the core boat

270   unlike unfrozen, saturated materials which tend to deform to fill the core boat. This can result in air gaps between the core and core boat. Figure 13 illustrates the relations between the core boat and core as well as a profile of the diamicton core (BS19-3-6). This core exhibits substantial rounding of the bottom that is not visible to the MSCL thickness laser, which only measures the core surface, resulting in local overrepresentation of core thickness and thus density measurement inaccuracy. Similarly, but less obvious, the ice-poor silt core appeared less dense because the upper ~5 cm of the core had a slight air gap

275   between the core and the core boat. Again, this gap is not detected by the laser measurements and results in an inaccurate measurement of the bulk density. This source of error underscores the importance of core preparation and positioning prior to scanning.

Although the peat core had a relatively consistent shape, the underside of the core did show minor variations in thickness. The impact of these differences is not immediately evident in the MSCL bulk density measurements. However,

280   these differences are amplified in the ice content estimates. As seen in Figure 10, the ice content data between 14-20 cm depth increases close to, and in some areas slightly above, 100%. These values coincide with the lowest recorded bulk densities in the profile and reflect the influence of small gaps between the core and the core boat. These gaps would have less impact on a core with a higher overall bulk density while they considerably affect ice content estimations of ice-rich material with low bulk density.

285   Another source of error in density measurements can occur at core breaks. The ice-rich organic silt core contains a core break, which is reflected in the data (Fig. 6). At 10 cm depth, the core break results in a higher density peak and thus a lower ice content estimate. The density peak associated with the core break occurs because the MSCL laser thickness records a decrease in core thickness while the gamma ray spot size overlaps the core break. The slight decrease in counts per second combined with a large decrease in core thickness at the core break compound to create an inference in the model toward

290   higher density, and thus lower ice content.

## 4.2 Within Core Transitions

Variations in grain size, ice content, and organic content can mark sharp changes in core cryostratigraphy, which can be observed in the gamma attenuation or in the magnetic susceptibility data. The transition core (Fig. 7) highlights the MSCL

ability to detect sharp changes in bulk density/ice content related to cryostratigraphic changes. At 8 cm depth the transition

295 core's sharp change is observed in the MSCL results as a rapid, sustained increase in bulk density from 0.9 g/cm$^3$ to ~1.6 g/cm$^3$. At the same time, the cuboid samples in this area fell on either side of the transition resulting in a sharp increase in bulk density between the 6-8 cm and 8-10 cm cuboids. Whereas in the diamict and ice-rich silt cores, this may not always be the case and sharp changes in density may be smoothed by the lower resolution cuboid sampling. The gradual increase observed in the gamma attenuation density results within the transition core can be related to the diameter of the gamma

300 beam relative to the acquisition resolution. In other words, a measurement was collected every 5 mm, but the diameter of the area covered by every measurement was ~10 mm resulting in averaging between neighbouring data points. Therefore, if a sharp local density high (ice-poor sediment layer) or density low (ice layer) occupies less than 10 mm of the vertical profile the density contrast across the boundary will be slightly muted. A good example of this is the ice layer in the ice-rich silt core at ~6 cm depth. This ice layer is picked up by the gamma attenuation sensor, although the lowest density recorded

305 across the ice layer is ~1.1 g/cm$^3$, suggesting that the surrounding sediment was still influencing the attenuation of the gamma while in the center of the ice layer. By contrast the destructive cuboid method shows no record of the ice layer in terms of a relative density low.

### 4.3 Impact of Inaccurate Soil Density Measurements on Non-destructive VIC Estimates.

Estimates of ice content are dependent on accurate, spatially resolved measurements of bulk density and an estimation of soil

310 density. For example, between 8-12 cm depth, the transition core differs from the cuboid ice content measurements and the MSCL equation results. This is caused by a local spike in the soil density due to a sand dominated layer. This was confirmed visually using the MSCL line-scan image of the core and can be observed in the bulk density measurements from the cuboid data near these depths (Fig. 7). The magnetic susceptibility also records a local high indicating the presence of minerals with high magnetization potential amongst the coarser sediments.

315 This scale of stratigraphic variation can be picked up with visual inspections of the MSCL core images and complementary datasets while maintaining a non-destructive approach to estimating ice content. It should be noted that the volumetric ice content data are calculated based on average soil density and therefore represent an estimation rather than a measurement. Nonetheless, this non-destructive method for estimating volumetric ice content is in close agreement with the cuboid results and only requires an estimate of the average soil density.

320 ### 4.4 Future Implications for Application of MSCL on Permafrost Cores.

The overall agreement between the cuboid and MSCL results shown in Figures 11 and 12 illustrate the MSCL's ability to be a reliable and accurate non-destructive method for collecting bulk density measurements from a wide variety of frozen materials. In addition to the higher resolution the MSCL provides, relative to most destructive methods, it also can collect data from tens of meters of core in a single day (depending on sampling resolution) while leaving the sample

325  uncompromised for future investigations. This represents a significant time savings in comparison to traditional destructive methods.

A benefit of the MSCL for permafrost applications is the development of digital archives detailing fundamental physical properties of previously collected permafrost cores. Permafrost cores are collected typically from remote locations at great expense and usually completely consumed in the analysis of physical properties. A digital archive containing high

330  quality data including ice content, bulk density, magnetic susceptibility, and high-resolution imagery provides an important resource for future permafrost investigations. This includes the retention of information from permafrost affected sites which may experience complete thaw in the coming years.

## 5 Conclusions

Ice content is a critical variable when considering the impact of thawing permafrost in the context of climate change. There

335  is a clear need to develop rapid, non-destructive methods to quantify ice content from a range of depositional settings to evaluate landscape responses to warming temperatures. Relative to previous destructive methods, MSCL provides a fast, non-destructive method for collecting high resolution bulk density measurements and volumetric ice content estimations from permafrost cores. The development of the MSCL method and redesigned frozen calibration piece, presented in this study, allows for accurate bulk density measurement to be collected at resolutions approaching 0.5 cm, while measuring

340  cores at ~2-3 cm per minute. We demonstrate a rapid approach to estimate the volumetric ice content using a combination of the bulk density from the gamma density measurements and measured soil density. The results compare well with traditional destructive methods demonstrating the potential of this method. The continued development and implementation of the MSCL within the permafrost community would greatly aid in the transition to a formal standardized method for collecting physical properties from permafrost cores and ultimately robust permafrost borehole digital archives.

## Author contribution

JP, DF, and AM planned the project; JP, AA, and CB collected the samples; JP, AM, and JH developed the methods; JP, AM, and JH performed the measurements; JP, MH, and JH analyzed the data; JP, AM, and MH wrote the manuscript draft; JP, MH, AM, JH, AA, CB, and DF reviewed and edited the manuscript.

## Competing interests

350  The authors declare that they have no conflict of interest.

**References**

360 Andersland, O. B., & Ladanyi, B. (1994). Frozen Ground. An Introduction to Frozen Ground Engineering, 1–22. https://doi.org/10.1007/978-1-4757-2290-1_1

ASTM. D4083–89 Standard test method for description of frozen soils (reapproved 2016). In. ASTM International: PA, USA; 2016. https://doi.org/10.1520/d4083

Bandara, S., Froese, D. G., St. Louis, V. L., Cooke, C. A., & Calmels, F. (2019). Post Depositional Mercury Mobility in a 365 Permafrost Peatland from Central Yukon, Canada. ACS Earth and Space Chemistry, 3(5), 770–778. https://doi.org/10.1021/acsearthspacechem.9b00010

Calmels, F., & Allard, M. (2004). Ice segregation and gas distribution in permafrost using tomodensitometric analysis. Permafrost and Periglacial Processes, 15(4), 367–378. https://doi.org/10.1002/ppp.508

Carbonneau, A., Allard, M., L'Herault, E., and LeBlanc, A., 2011. High permafrost ice contents in Holocene slope deposits 370 as observed from shallow geophysics and a coring program in Pangnirtung, Nunavut, Canada. In Proceedings of AGU Fall Meeting 2011: American Geophysical Union, Fall Meeting 2011, abstract id. C41C-0419.

Darrow, M. M., & Lieblappen, R. M. (2020). Visualizing cation treatment effects on frozen clay soils through μCT scanning. Cold Regions Science and Technology, 175, 103085. https://doi.org/10.1016/j.coldregions.2020.103085

Evans, H.B., 1965. GRAPE - A device for continuous determination of material density and porosity. In: Proceedings of 6th 375 Annual SPWLA Logging Symposium. 2. Dallas, TX. pp. B1-B25

Fortin, D., Francus, P., Gebhardt, A. C., Hahn, A., Kliem, P., Lisé-Pronovost, A., Roychowdhury, R., Labrie, J., & St-Onge, G. (2013). Destructive and non-destructive density determination: method comparison and evaluation from the Laguna Potrok Aike sedimentary record. Quaternary Science Reviews, 71, 147–153. https://doi.org/10.1016/j.quascirev.2012.08.024

Geotek, LTD., 2021. Multi-sensor Core Logger manual. Daventry, United Kingdom. Need to add date of last update

380    Gunn, D. E., & Best, A. I. (1998). A new automated nondestructive system for high resolution multi-sensor core logging of open sediment cores. Geo-Marine Letters, 18(1), 70–77. https://doi.org/10.1007/s003670050054.

Heiri, O., Lotter, A.F. and Lemcke, G., 2001. Loss on ignition as a method for estimating organic and carbonate content in sediments: reproducibility and comparability of results. Journal of paleolimnology, 25(1), pp.101-110. https://doi.org/10.1023/A:1008119611481.

385    Hunt, J. E., Wynn, R. B., Masson, D. G., Talling, P. J., & Teagle, D. A. H. (2011). Sedimentological and geochemical evidence for multistage failure of volcanic island landslides: A case study from Icod landslide on north Tenerife, Canary Islands. Geochemistry, Geophysics, Geosystems, 12(12), n/a-n/a. https://doi.org/10.1029/2011gc003740

Jorgenson, M.T., Romanovsky, V., Harden, J., Shur, Y., O'Donnell, J., Schuur, E.A.G., Kanevskiy, M. and Marchenko, S. (2010). Resilience and vulnerability of permafrost to climate change. Canadian Journal of Earth Sciences, 40: 1219-1236.

390    https://doi.org/10.1139/X10-060

Kokelj, S. V., & Burn, C. R. (2003). Ground ice and soluble cations in near-surface permafrost, Inuvik, Northwest Territories, Canada. Permafrost and Periglacial Processes, 14(3), 275–289. https://doi.org/10.1002/ppp.458

Kleinberg, R. L., & Griffin, D. D. (2005). NMR measurements of permafrost: unfrozen water assay, pore-scale distribution of ice, and hydraulic permeability of sediments. Cold Regions Science and Technology, 42(1), 63–77.

395    https://doi.org/10.1016/j.coldregions.2004.12.002

Kuras, O., Shreeve, J., Smith, N., Graham, J and Atherton, N. (2016). Enhanced Characterisation of Radiologically Contaminated Sediments at Sellafield by MSCL Core Logging and X-ray Imaging. In Near Surface Geoscience 2016-22nd European Meeting of Environmental and Engineering Geophysics (Vol. 2016, No. 1, pp. cp-495). European Association of Geoscientists & Engineers. https://doi.org/10.3997/2214-4609.201601918

400    Kruse, A. M., & Darrow, M. M. (2017). Adsorbed cation effects on unfrozen water in fine-grained frozen soil measured using pulsed nuclear magnetic resonance. Cold Regions Science and Technology, 142, 42–54. https://doi.org/10.1016/j.coldregions.2017.07.006

Lenz, J., Grosse, G., Jones, B. M., Walter Anthony, K. M., Bobrov, A., Wulf, S., & Wetterich, S. (2015). Mid-Wisconsin to Holocene Permafrost and Landscape Dynamics based on a Drained Lake Basin Core from the Northern Seward Peninsula,

405    Northwest Alaska. Permafrost and Periglacial Processes, 27(1), 56–75. Portico. https://doi.org/10.1002/ppp.1848

Linell, K. A. and Kaplar, C. W. (1966), Description and classification of frozen soils, U.S. Army Cold Reg. Res. Eng. Lab. Tech. Rep. 140.

Lin, Z., Gao, Z., Fan, X., Niu, F., Luo, J., Yin, G., & Liu, M. (2020). Factors controlling near surface ground-ice characteristics in a region of warm permafrost, Beiluhe Basin, Qinghai-Tibet Plateau. Geoderma, 376, 114540.

410    https://doi.org/10.1016/j.geoderma.2020.114540

Liu, H., Maghoul, P., Shalaby, A., & Thomson, D. (2023). Ultrasonic characterization of frozen soils using a multiphase poromechanical approach. Computers and Geotechnics, 153, 105068. https://doi.org/10.1016/j.compgeo.2022.105068

Niessen, F., Magens, D. and Gebhardt, A.C. (2007). Physical properties of the AND-1B Core, ANDRILL McMurdo ice shelf project, Antarctica. Terra Antartica, 14(3), pp.155-166 hdl:10013/epic.30000.d001

415 Pihlainen, J.A. and Johnston, G.H., 1963. Guide to a field description of permafrost. National Research Council Canada, Associate Committee on Soil and Snow Mechanics, Ottawa, Technical Memorandum No. 79, 21 p.

Smol, J. P., Birks, H. J. B., & Last, W. M. (Eds.). (2001). Tracking Environmental Change Using Lake Sediments. Developments in Paleoenvironmental Research. https://doi.org/10.1007/0-306-47671-1

Stephani, E., Fortier, D., Shur, Y. (2010). Applications of cryofacies approach to frozen ground engineering – case study of a
420 road test site along the Alaska highway (Beaver Creek, Yukon, Canada). Joint 63rd Canadian geotechnical conference and 6th Canadian permafrost conference; Calgary, Canada. https://doi.org/10.13140/2.1.2467.2961

Throop, J., Lewkowicz, A. G., & Smith, S. L. (2012). Climate and ground temperature relations at sites across the continuous and discontinuous permafrost zones, northern Canada. Canadian Journal of Earth Sciences, 49(8), 865–876. https://doi.org/10.1139/e11-075.

425 Vardy, M. E., L'Heureux, J.-S., Vanneste, M., Longva, O., Steiner, A., Forsberg, C. F., Haflidason, H., & Brendryen, J. (2012). Multidisciplinary investigation of a shallow near-shore landslide, Finneidfjord, Norway. Near Surface Geophysics, 10(4), 267–277. Portico. https://doi.org/10.3997/1873-2012022

Weber, M. E., Niessen, F., Kuhn, G., & Wiedicke, M. (1997). Calibration and application of marine sedimentary physical properties using a multi-sensor core logger. Marine Geology, 136(3–4), 151–172. https://doi.org/10.1016/s0025-
430 3227(96)00071-0

Zhou, X., Zhou, J., Kinzelbach, W., & Stauffer, F. (2014). Simultaneous measurement of unfrozen water content and ice content in frozen soil using gamma ray attenuation and TDR. Water Resources Research, 50(12), 9630–9655. Portico. https://doi.org/10.1002/2014wr015640
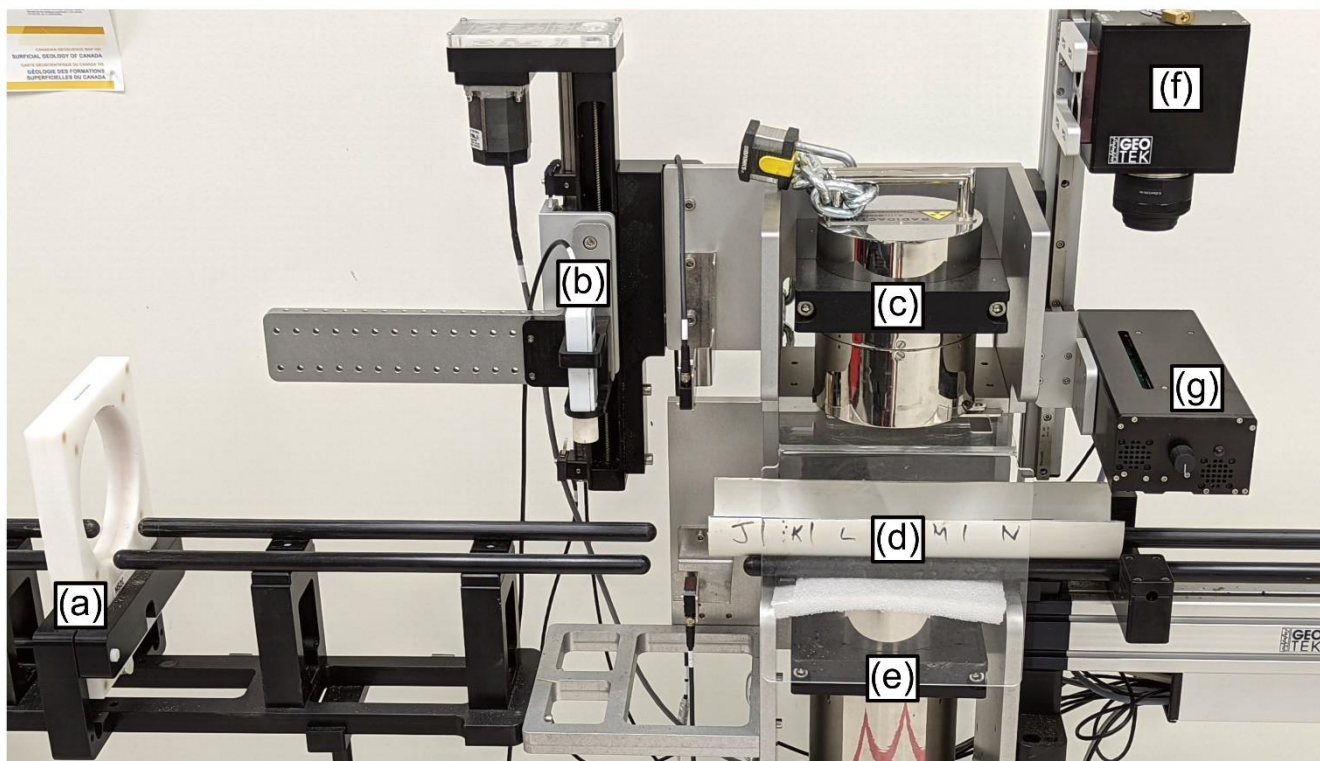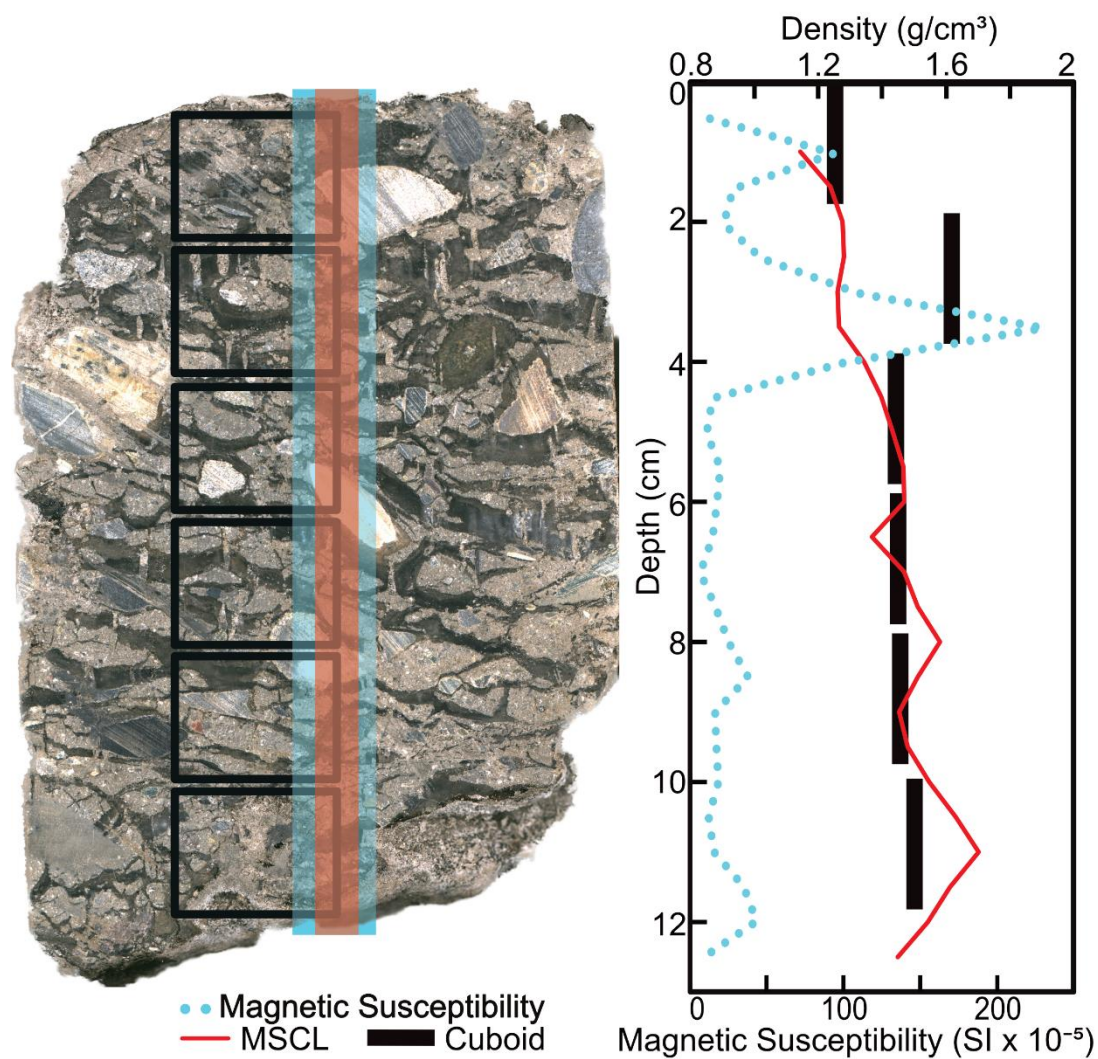
**Figure 1: The PACS Laboratory MSCL is equipped with the following components: (a) loop magnetic susceptibility sensor, (b) point magnetic susceptibility sensor, (c) Caesium-137 ($^{137}$Cs) gamma ray source, (d) core boat (40 cm in length) (e) gamma detector, (f) imaging camera box, and (g) camera light box.**
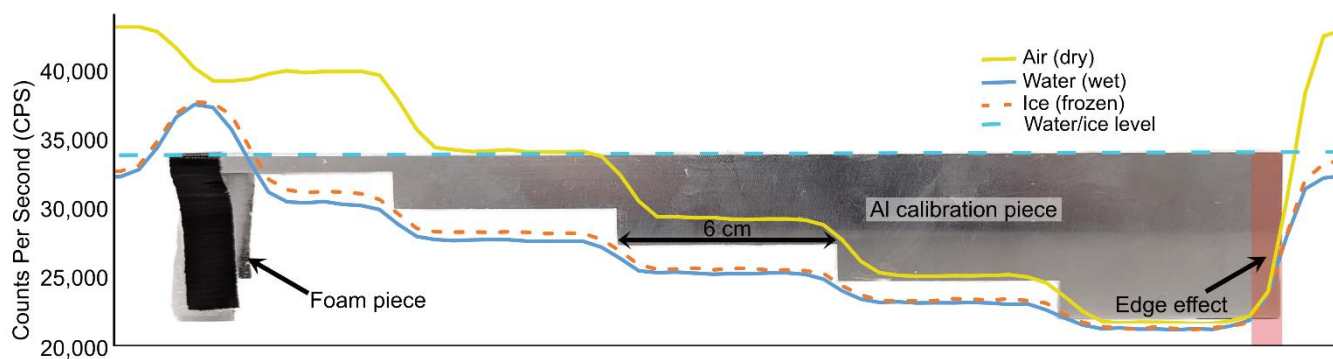


**Figure 2: Comparison of the wet, frozen (ice) and dry calibration of gamma density.**

17

**Figure 3: Image of a core highlighting the destructive subsample (cuboid) locations (in black) relative to the non-destructive data paths of the MSCL transects.**

445

18
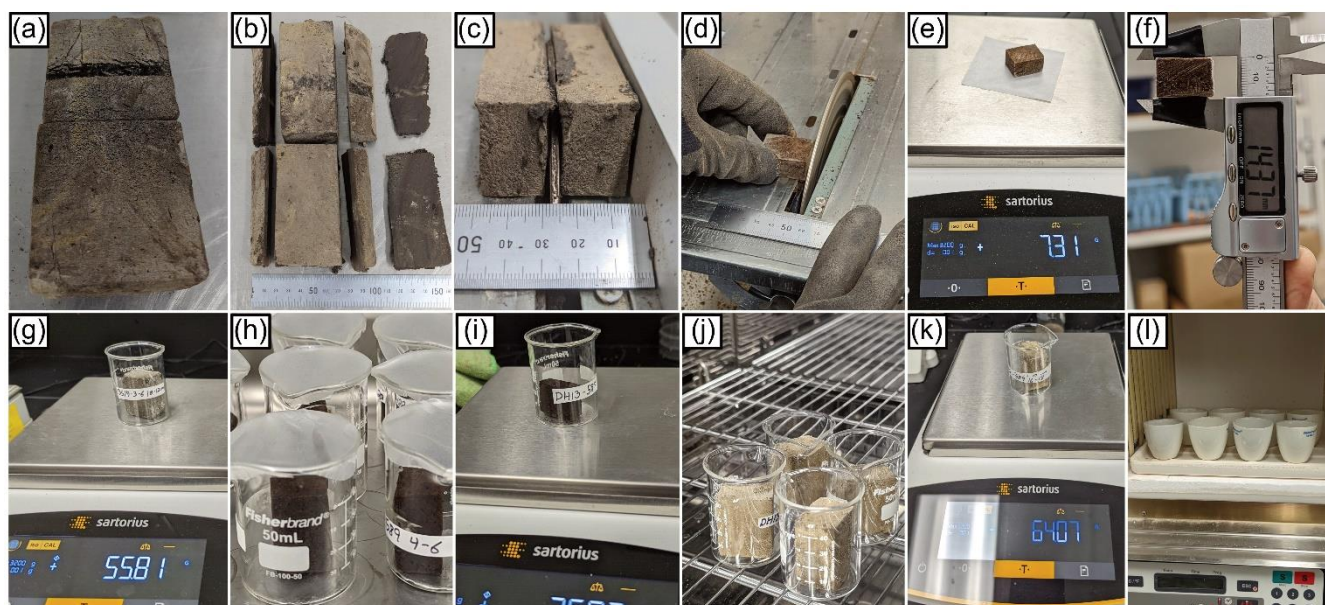
**Figure 4: Images of the cuboid method as implemented for this study.**

**Table 1: Sampling location and physical properties of cores analyzed in the study. Soil densities were measured via the cuboid method.**

| Core ID | Length (cm) | Classification/Properties | Collection Location | Cuboid measured Soil Density (g/cm³) |
|---------|-------------|---------------------------|---------------------|--------------------------------------|
| BH19-204 | 21 | Ice-wedge | Alaska HWY, Yukon, Canada | N/A |
| BH18-211 | 23 | Ice-rich silt | Alaska HWY, Yukon, Canada | 2.02 (n=20) |
| BH12F-138 | 16 | Transition between ice-rich silty peat and ice-poor inorganic silt | Alaska HWY, Yukon, Canada | 1.29 (top; n=8) 2.17 (bottom; n=8) |
| BS19-3-6 | 19 | Diamicton | Dempster HWY, Yukon, Canada | 2.44 (n=12) |
| BH20B-337 | 20 | Ice-poor silt | Alaska HWY, Yukon, Canada | 2.67 (n=18) |
| DH13-589 | 26 | Ice-rich homogenous peat. | Dempster HWY, Yukon, Canada | 1.44 (n=24) |
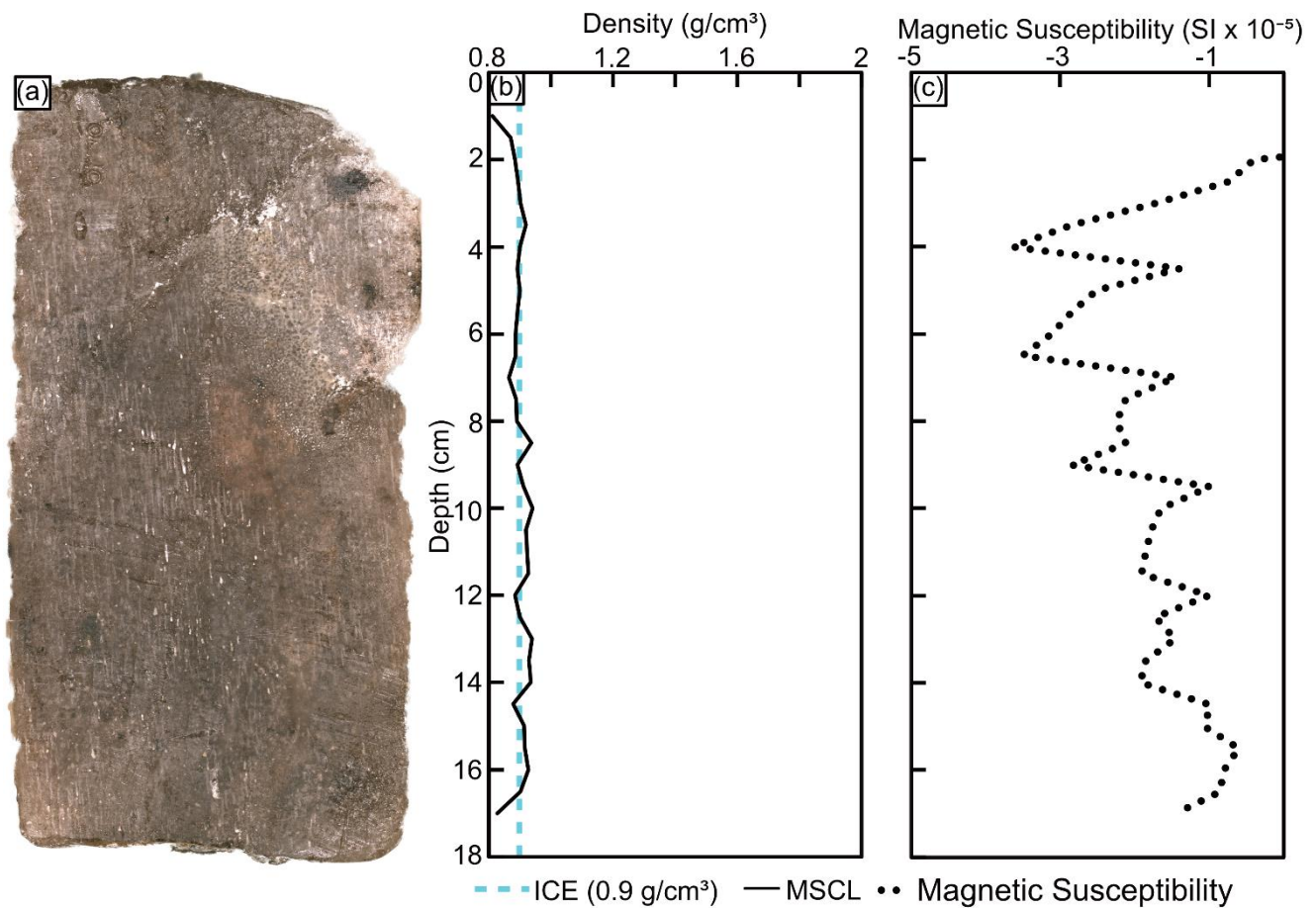
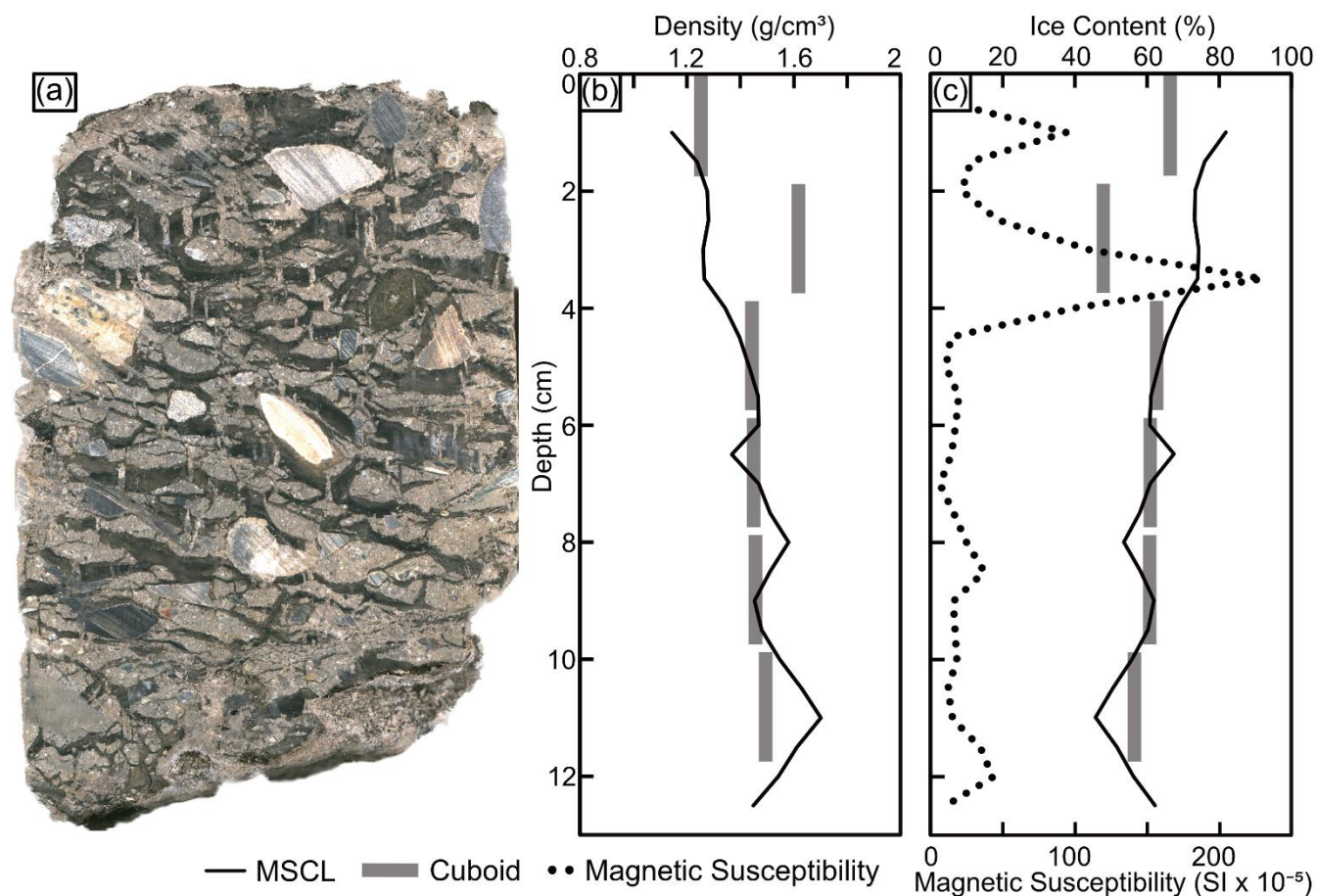Figure 5: (a) MSCL image of the ice-wedge core; (b) gamma attenuation density; (c) magnetic susceptibility.
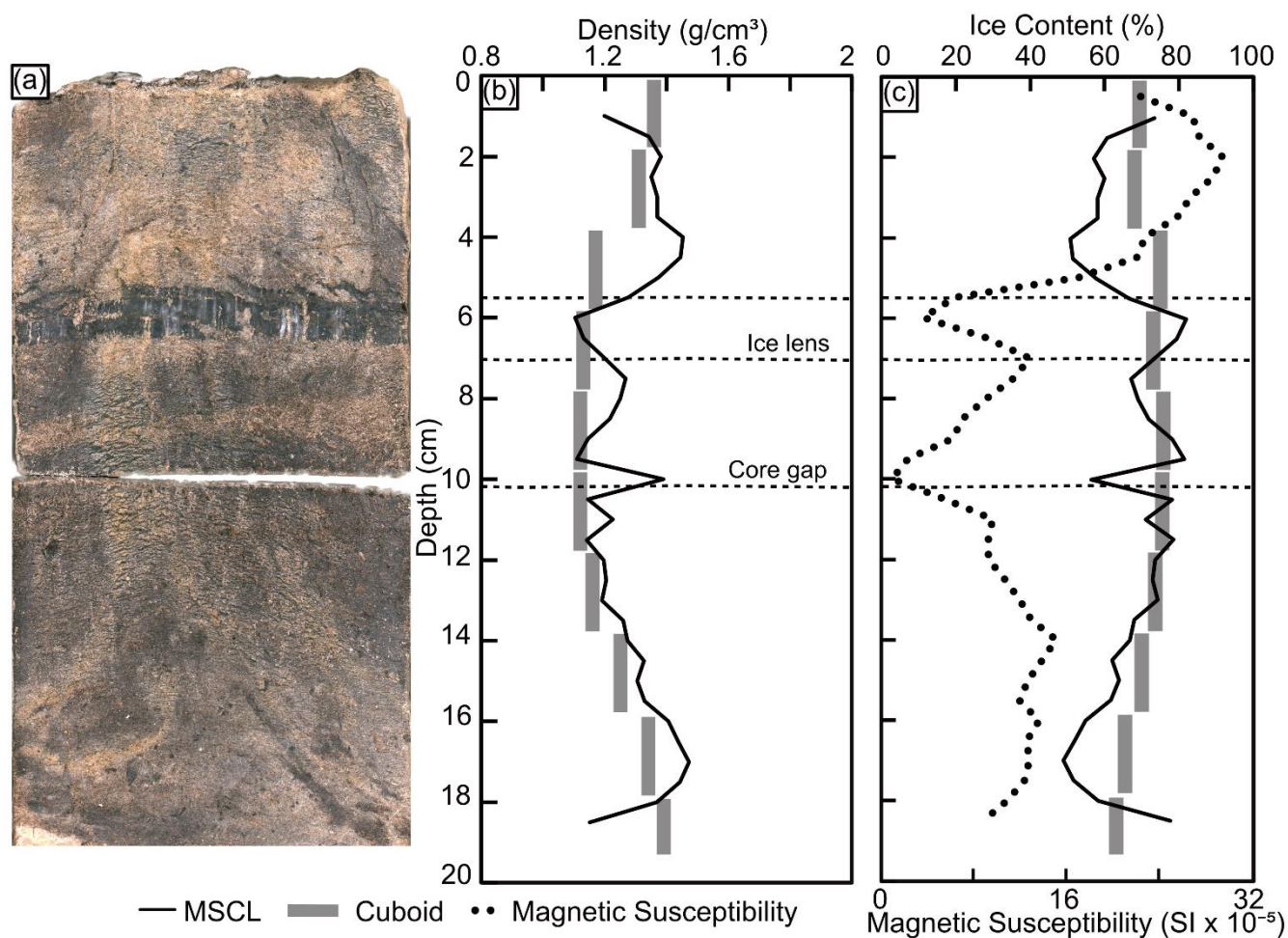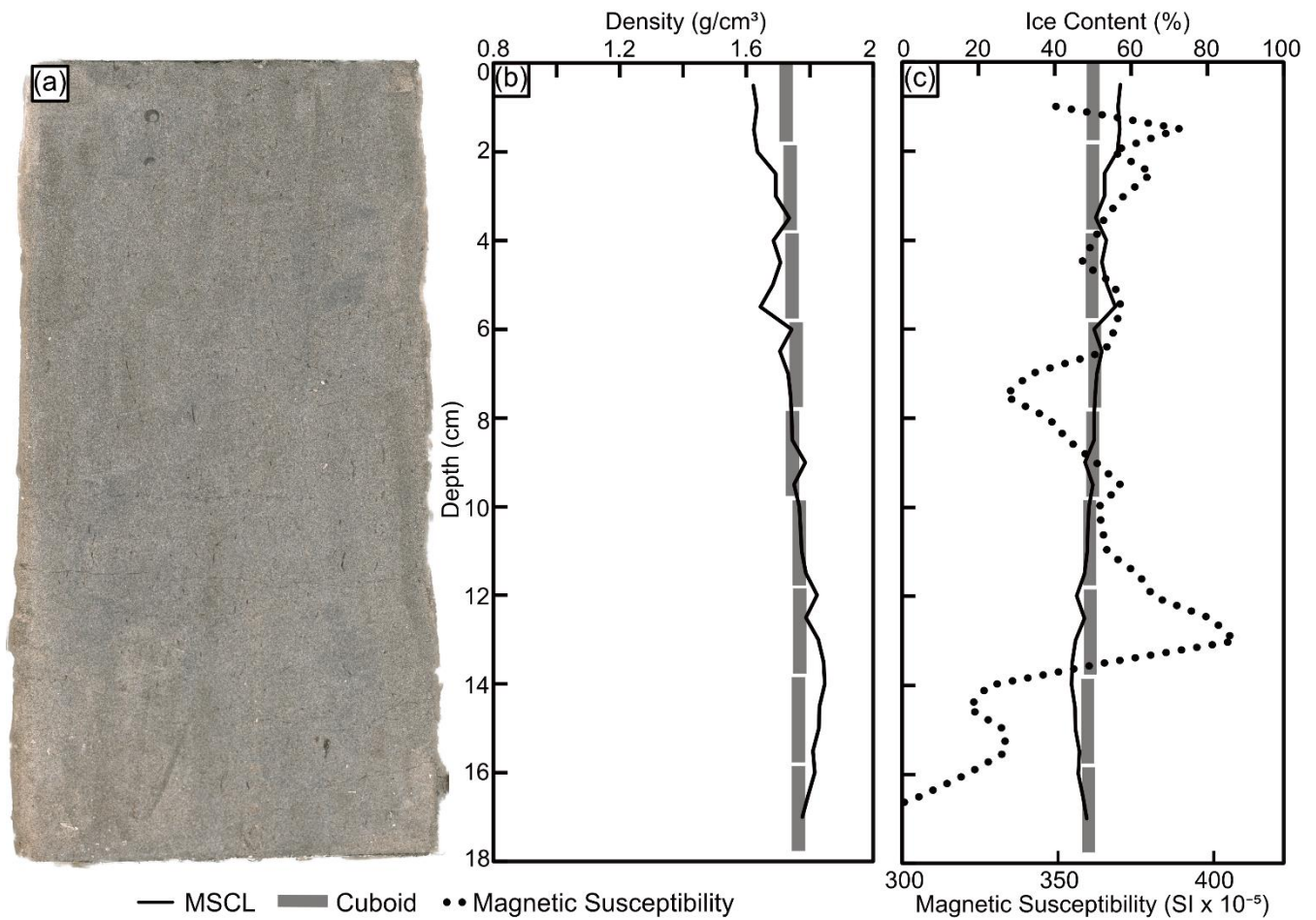
**Figure 6: (a) MSCL image of ice-rich silt core; (b) bulk density comparison between gamma attenuation and cuboid data; (c) estimated volumetric ice content from bulk density and cuboid, and magnetic susceptibility data.**
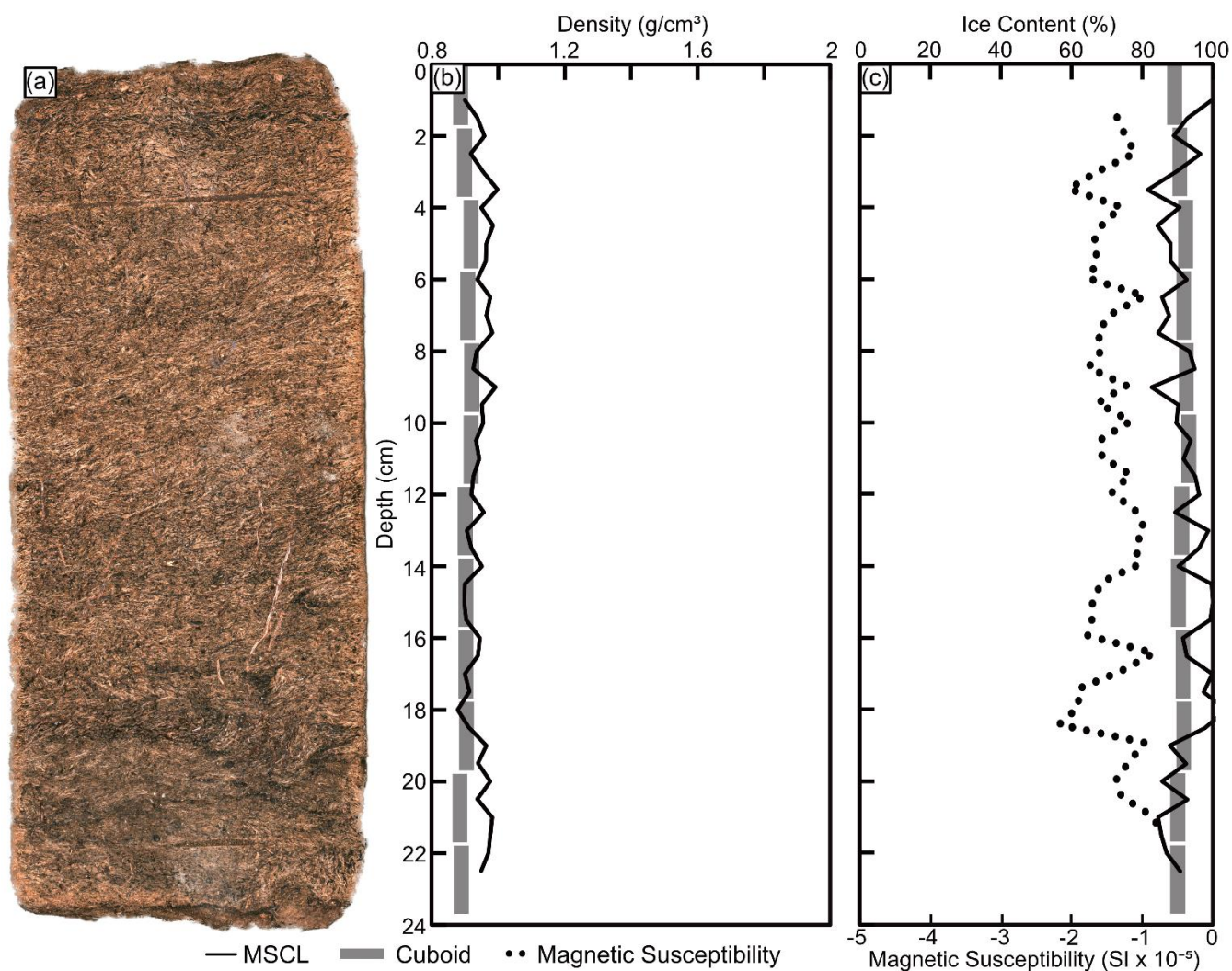
455
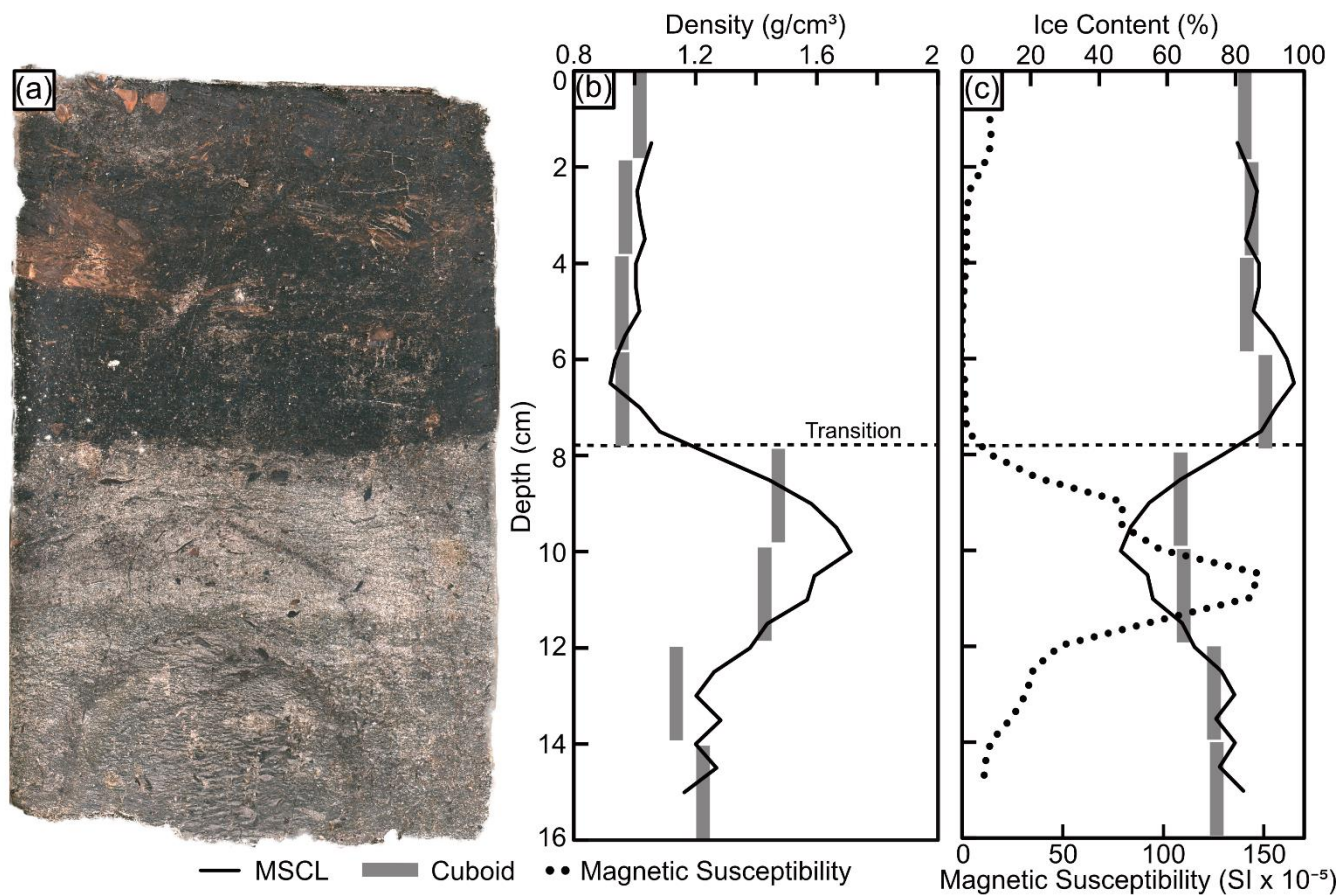
Figure 7: (a) MSCL image of transition core; (b) bulk density comparison between gamma attenuation and cuboid data; (c) estimated volumetric ice content from gamma attenuation bulk density, cuboid ice content and magnetic susceptibility data.

**Figure 8: (a) MSCL image of diamicton core; (b) bulk density comparison between gamma attenuation and cuboid data; (c) estimated volumetric ice content from gamma attenuation bulk density, cuboid ice content and magnetic susceptibility data.**

**Figure 9: (a) MSCL image of ice-poor silt core; (b) bulk density comparison between gamma attenuation and cuboid data; (c) estimated volumetric ice content from gamma attenuation bulk density, cuboid ice content and magnetic susceptibility data.**
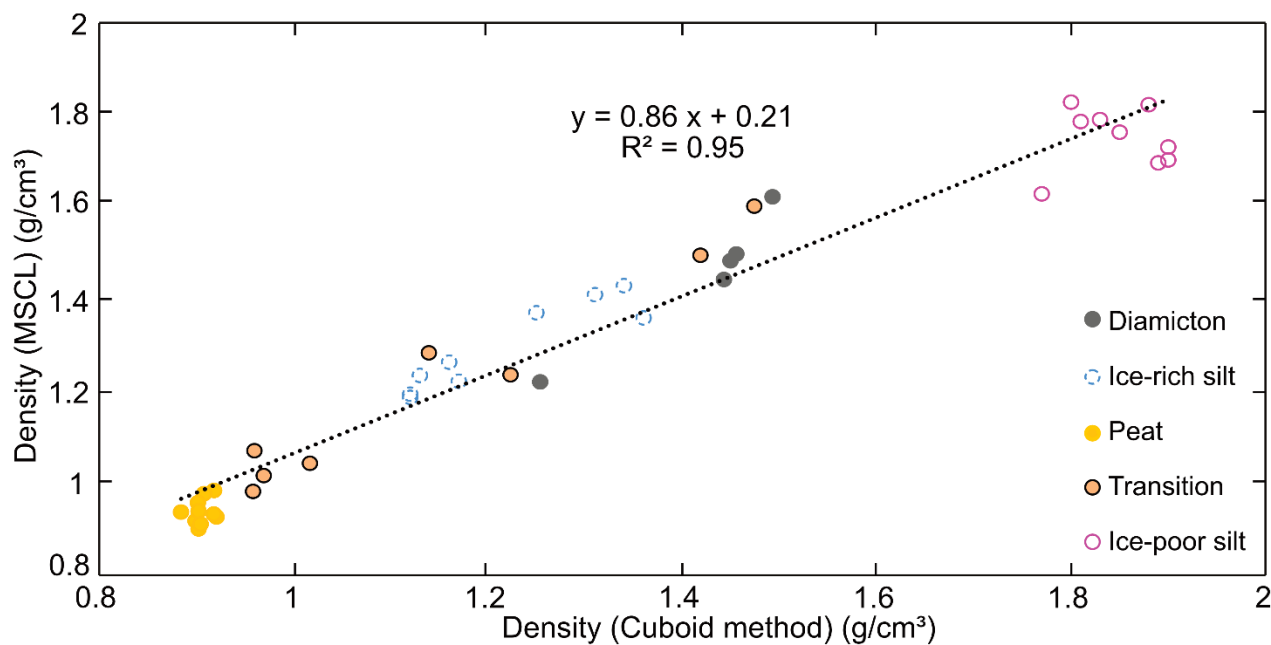
470

**Figure 10: (a) MSCL image of peat core; (b) bulk density comparison between gamma attenuation and cuboid data; (c) estimated volumetric ice content from gamma attenuation bulk density, cuboid ice content and magnetic susceptibility data.**

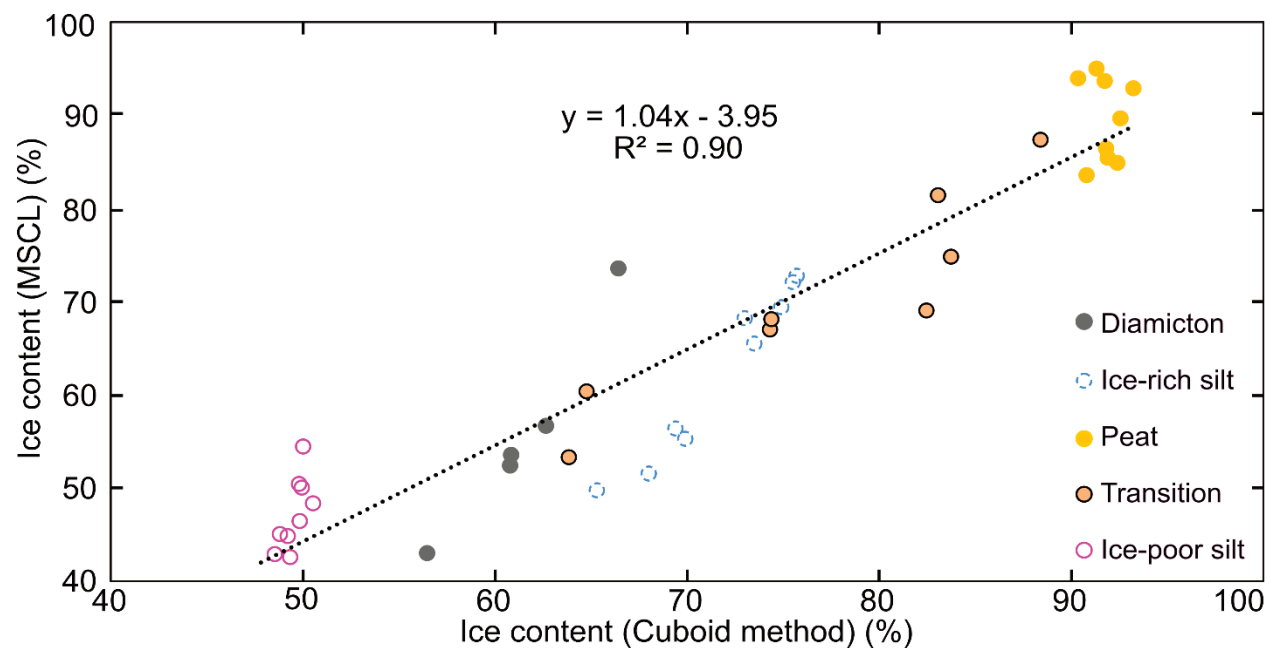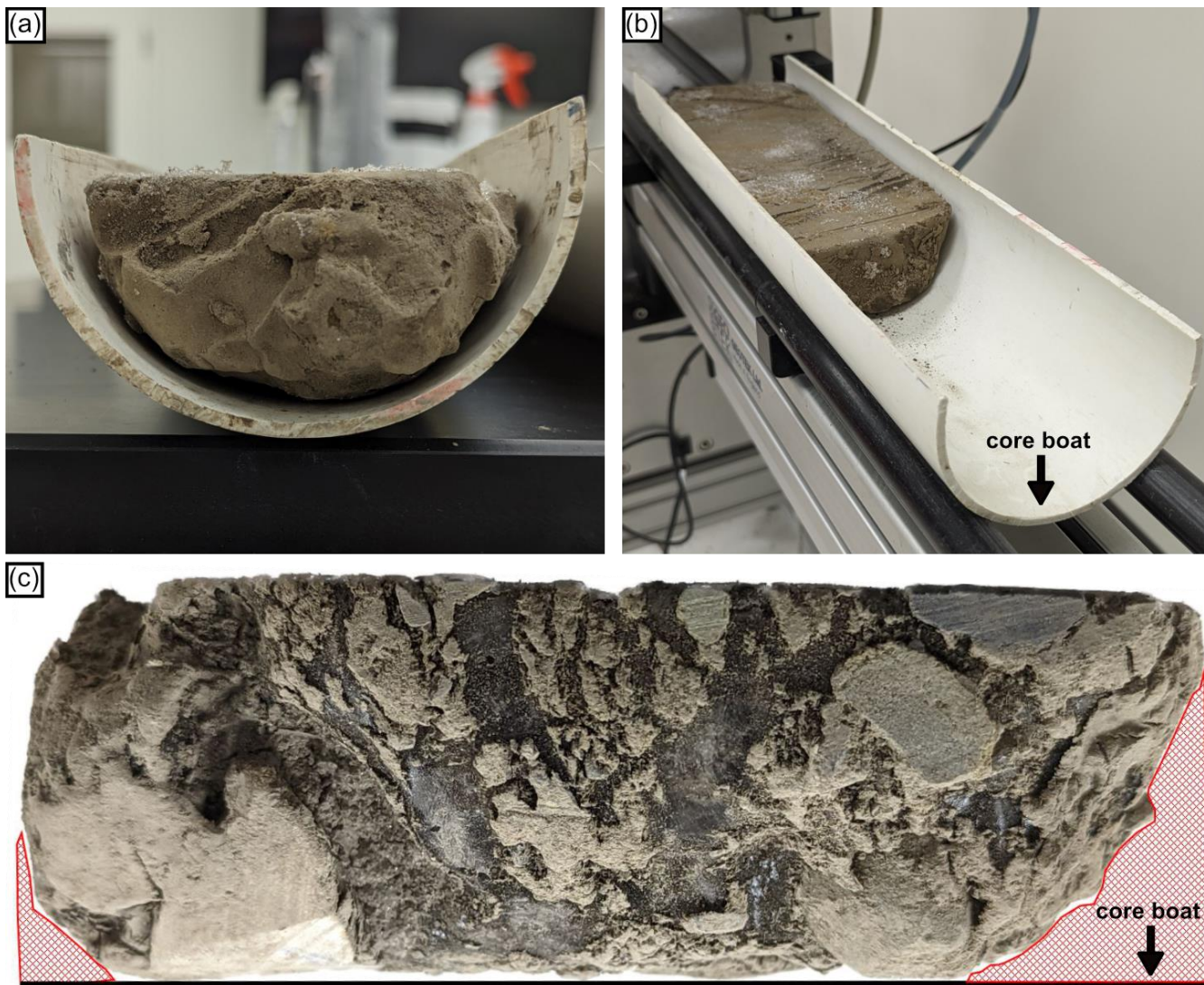**Figure 11: Comparison between the bulk density data for the cuboid method and the MSCL.**

475



**Figure 12: Comparison between volumetric ice content results from the cuboid and estimates from the MSCL.**

**Figure 13: The MSCL core boat and core positioning examples; (a) down core view of a core in the core boat with minimal air gaps; (b) photo of core in the core boat on the MSCL track; (c) diamicton core (BS19-3-6) side profile to highlight the thickness variation not visible to the MSCL laser.**